3D Visualisation of trans-syncytial nanopores provides a pathway for paracellular diffusion across the human placental syncytiotrophoblast

Short title: Trans-syncytial nanopores

Rohan M Lewis*[1,3], Harikesan Baskaran[4], Jools Green[1], Stanimir Tashev[2], Eleni Paleologou[1], Emma M Lofthouse[1], Jane K Cleal[1,3], Anton Page[2], David S Chatelet[2], Patricia Goggin[2], Bram G Sengers[3,4]

[1] University of Southampton, Faculty of Medicine

[2] University of Southampton, Faculty of Medicine, Biomedical Imaging Unit

[3] University of Southampton, Institute for Life Sciences

[4] University of Southampton, Faculty of Engineering and Physical Sciences

***Corresponding Author**: Rohan M Lewis, MP 887, IDS Building University of Southampton, Faculty of Medicine, Southampton General Hospital, rohan.lewis@soton.ac.uk

Abstract

The placental syncytiotrophoblast, a syncytium without cell-cell junctions, is the primary barrier between the mother and the fetus. Despite no apparent anatomical pathway for paracellular diffusion of solutes across the syncytiotrophoblast size-dependent paracellular diffusion is observed. Here we report data demonstrating that the syncytiotrophoblast is punctuated by trans-syncytial nanopores (TSNs). These membrane-bound TSNs directly connect the maternal and fetal facing sides of the syncytiotrophoblast, providing a pathway for paracellular diffusion between the mother and fetus. Mathematical modelling of TSN permeability based on their 3D geometry suggests that 10-37 million TSNs per cm^3 of placental tissue could explain experimentally observed placental paracellular diffusion. TSNs may mediate physiological hydrostatic and osmotic pressure homeostasis between the maternal and fetal circulations but also expose the fetus to pharmaceuticals, environmental pollutants and nanoparticles.

Introduction

The placenta was once viewed as a perfect barrier, but as the thalidomide tragedy demonstrated, this is not the case [1]. It is now clear that potentially harmful molecules and particulates can cross the placenta and adversely affect fetal development. However, the mechanism by which these molecules and particulates cross the placenta is not always clear [2, 3]. Understanding how these substances cross the placenta is necessary to identify the risks and prevent long-term consequences of these exposures, which may adversely affect fetal and postnatal health [4].

The primary placental barrier is the syncytiotrophoblast, a continuous syncytial monolayer covering the villi at the maternal-fetal interface. As there are no cell-cell junctions in a syncytium, there is no obvious pathway by which paracellular diffusion can occur. Despite the absence of an anatomical pathway for diffusion, there is physiological evidence for size-dependent paracellular diffusion of solutes [5, 6]. Trans-syncytial channels, or nanopores, have been proposed as mediators of trans-syncytial diffusion, however continuous full-width nanopores have not been previously demonstrated in the human placenta [7]. An alternative hypothesis to explain paracellular diffusion is that it occurs through regions of syncytial damage [8]. These hypotheses are not mutually exclusive but establishing mechanisms of fetal exposure is necessary to understand the likely risks of different compounds and develop strategies to mitigate this.

Selective placental transfer of nutrients, IgG, wastes and exogenous toxins is facilitated by membrane transporters and endocytosis [9-11]. However it is not clear how exogenous drugs and toxins reach the fetus as, with a few exceptions such as the apically located exchanger OATP4A1 [10], drug transporters in the placenta mediate efflux from the fetus to the mother [12]. Nanoparticle transfer across the placenta has been observed, but the mechanism is unclear [13]. A more extensive understanding of how metabolites, pharmaceuticals and toxins reach the fetal circulation is necessary to protect fetal health.

Estimates of placental permeability surface area products for hydrophilic solutes have been determined *in vivo* and show size-dependent permeability of solutes, which decreases with increasing molecular radius [5, 6]. In other species with haemochorial placentas, permeability has also been shown to be size-selective with some species having higher or lower overall permeability compared to humans [3, 14]. This data suggests a size-selective permeability of the placenta through low diameter channels [15].

Using serial block-face scanning electron microscopy (SBF SEM) to reconstruct placental ultrastructure in three dimensions, this study demonstrates the presence of full-width trans-syncytial nanopores (TSNs) in the human placenta.

Methods

Term placental tissue was collected after delivery from uncomplicated pregnancies with written informed consent and ethical approval from the Southampton and Southwest Hampshire Local Ethics Committee (11/SC/0529). Villous samples from 8 placentas were processed and imaged using TEM or SBFSEM as described previously [27]. Regions containing TSNs were manually segmented in Avizo v2019.4 (ThermoFisher, Eindhoven).

Modelling of nanopore diffusive transfer capacity

The nanopore diffusive transfer capacity for a particular molecule is determined by its diffusivity in free solution as well as the geometry of the pore, specifically the pore length and cross sectional area. Here we will calculate this geometric contribution in the form of the effective area-over-length ratio A_{pore}/L_{pore} [m], which is a measure for the effect of pore geometry on diffusive transfer, independent of the solute studied. This parameter can then be used to calculate nanopore diffusive transfer using the concentration gradient and diffusion coefficient for any specific solute.

Briefly, the magnitude of the diffusive flux J_{pore} [mol/s] through a pore of uniform cross section is given by:

$$J_{pore} = DA_{pore}\frac{|\Delta C|}{L_{pore}} \qquad \text{Eq. 1}$$

where D [m^2/s] is the diffusion coefficient, A_{pore} [m^2] the pore cross sectional area, ΔC [mol/m^3] the concentration difference over the pore and L_{pore} [m] the pore length. This can also be expressed in terms of the permeability surface area product PS_{pore} [m^3/s]:

$$J_{pore} = PS_{pore}\Delta C \quad \text{, where } PS_{pore} = \frac{DA_{pore}}{L_{pore}} \qquad \text{Eq. 2}$$

Since in reality the pore cross sectional area is not uniform, 3D image-based modelling was used to calculate the effective area-over-length ratio A_{pore}/L_{pore} [m] based on Eq. 1 by prescribing the concentration difference and diffusivity and then monitoring the resulting flux in the simulations. Segmented image stacks were imported in Simpleware ScanIP (P-2019.09; Synopsys, Inc., Mountain View, USA). Voxels were resampled isotropically so that the x and y pixel size matched the z axis spacing. Pores were meshed using linear tetrahedral elements. Different coarseness settings were evaluated to establish convergence, with the final number of elements used for the different pores ranging from 1.4–38×10^5.

Steady state diffusion simulations were performed in COMSOL Multiphysics (v5.5; COMSOL AB, Stockholm, Sweden). Since A_{pore}/L_{pore} does not depend on the choice of parameters, $D = 1$ m^2/s was used and a fixed concentration gradient $\Delta C = 1$ mol/m^3 was imposed by constant concentration boundary conditions on the inlet and outlet surface of the pore , while the remaining external surface was subject to no-flux conditions.

After simulations, the magnitude of the diffusive flux J_{pore} given by the integral of the solute flux in the direction normal to the pore inlet or outlet taken over the inlet/outlet cross sectional area, was then used to calculate the effective pore area-over-length ratio A_{pore}/L_{pore} based on Eq. 1.

For a specific solute, the permeability surface area product for a single pore PS_{pore} was obtained by multiplying the average A_{pore}/L_{pore} value by the relevant diffusion coefficient (Eq. 2). The number of pores n_{pores} [g^{-1}] per gram of placental tissue was then estimated based on Eq. 3:

$$n_{pores} = \frac{PS_{placenta}}{PS_{pore}} \qquad \text{Eq. 3}$$

where $PS_{placenta}$ [$m^3\ s^{-1}\ g^{-1}$] is the overall experimentally observed placental permeability surface area product for the corresponding solute from literature.

Results

Trans-syncytial nanopores

This study manually inspected 14 SBFSEM image stacks from five different placentas to identify trans-syncytial nanopores (TSNs) defined as membrane lined pores connecting the apical and basal plasma membranes of the syncytiotrophoblast. These stacks consisted of 7487 SBFSEM images, representing a total volume of 0.00000017 cm^3.

Inspection of serial sections allowed identification of TSNs crossing the syncytiotrophoblast. Continuous TSNs with a clear connection between the apical and basal membranes were identified. Near-continuous TSNs were also identified which had connections to both the apical microvillous and basal plasma membranes but contained discontinuities along the length of the nanopore. Unilateral nanopores, ultrastructurally similar to TSNs but opened from either the apical or basal plasma membrane without connecting to the opposite membrane were identified. An illustration of these nanopore types as we defined then is shown in (figure 1). Regions containing TSNs were manually segmented in Avizo v2019.4 (ThermoFisher, Eindhoven). Cross section from one of these TSNs are shown in figure 2. The lumens of TSNs typically had low electron density, consistent with a primarily fluid filled pore (figure 2a, c and d). However, some TSNs and regions of TSNs were observed with higher electron density indicating diffuse contents (figure 2e). The nanopore shown in figure 2 can be seen reconstructed in 3D (Supplemental movie 1) and a movie showing the nanopore lumen highlighted in sequential sections (supplemental movie 2) can be seen in the supplemental material.

Ten continuous TSNs were identified from three different placentas and these did not have a uniform structure (figure 3). While the least complex TSNs were direct tubes connecting the apical and basal membranes (figure 3c) the most complex full width TSN was a double pore with two bifurcated apical openings (4 in total) and two basal openings (figure 3a). Blind ends are present in the TSNs shown in figure 2d, i and g.

In addition, 20 near-continuous TSNs were identified, with examples in all five placentas studied. In two cases, these near-continuous TSNs were highly complicated with branches, multiple dilations, and blind ends (figure 4b). Finally, 25 unilateral nanopores were identified arising from either the apical (n = 17) or basal (n = 8) plasma membrane of the syncytiotrophoblast but not connecting to the opposing plasma membrane.

On the basal membrane, continuous and near-continuous TSN were observed opening adjacent to basal lamina in 16 cases and regions adjacent to cytotrophoblast in 14 cases.

Of the ten continuous TSNs, eight contained membrane-bound inclusions which, surrounded by pore membrane, formed double-membrane structures (figure 4). Inclusions were also observed in the majority of near-continuous and unilateral nanopores. In three cases, the inclusions appeared to be trophoblastic in origin. In the first case, the inclusion on the apical side appeared to be connected to the syncytiotrophoblast by at least one thin stalk of cytoplasmic material (figure 4a-c). At the available resolution, it was not clear whether other inclusions were also engulfed syncytiotrophoblast. In two cases, an inclusion on the

basal side of the placenta was a clear-cut protrusion from an underlying cytotrophoblast cell (figure 4d-f).

Another less commonly observed feature associated with TSNs were thin nanopores within the syncytiotrophoblast, where two closely adjacent membranes were joined by desmosome like adhesions (figure 5). These were observed in two TEM images and one SBFSEM image stack. In one case a desmosome associated nanopore was seen almost crossing the placenta from the basal membrane to near the microvillous membrane (figure 5a). Desmosome associated nanopores were observed in one SBF SEM image stack where they were found to be ribbon or sheet-like structures 5-16 nm wide and estimated at 200-800 nm deep (figure 5b). Desmosome containing nanopores could be seen appearing and disappearing within the same 2D section, which is consistent with a pore rather than a cell-cell junction. Topologically a cell-cell junction would need to either interact with two cell or image boundaries or form a circular feature (figure 5c).

Modelling diffusion through TSNs

Depending on their geometry, individual nanopores display a large variation in estimated effective A_{pore}/L_{pore} from 0.14 x 10^{-8} m to 2.08 x 10^{-8} m (figure 2k). The effective A_{pore}/L_{pore} ratio based on the results of the computational simulations of the ten pores, as depicted in figure 2, was in the order of 10 nm (8.5 ± 7.2 × 10^{-9} m, mean ± SD). By multiplying the mean effective A_{pore}/L_{pore} ratio with the diffusion coefficient for particular solutes using Eq. 2, the average permeability surface area products for a single pore could then be calculated (table 1). Dividing the experimentally observed placental permeability surface area products (from the literature) by the average permeability surface area product for a single pore, resulted in placental pore number estimates between 13 and 37 million pores per gram.

Discussion

The demonstration of nanoscale pores punctuating the syncytiotrophoblast challenges our understanding of the placenta as a barrier. It suggests that rather than being a continuous physical barrier between mother and fetus, the syncytiotrophoblast is a molecular sieve facilitating diffusion of small solutes via active maintenance of TSNs. Computational modelling diffusion though these channels suggests that these solutes may include nutrients and toxins, so this transfer route may have profound implications for the fetus.

TSNs were structurally heterogeneous, including simple tubes, tubes with dilated regions and branched structures with blind ends. Many TSNs also contained inclusions of membrane-bound material, in three cases trophoblastic in origin but in most cases the origin was unclear. Some TSNs had multiple openings to the syncytiotrophoblast apical microvillous or basal membranes. The near-continuous and unilateral nanopores are likely in the process of formation, degradation or remodelling. It is also possible that near-continuous TSNs are continuous but that the connections were too thin to observe. The relatively large number of

191 near-continuous and unilateral nanopores is consistent with TSNs being dynamically
192 remodelled.
193 There was a wide range in calculated permeability parameters for the modelled TSNs,
194 with diffusion through the most permeable being 10 x greater than the least permeable. As
195 might be expected, shorter, wider TSNs had the greatest permeability while the longer TSNs
196 had the lowest permeability (excluding the TSN with multiple apical and basal openings).
197 The time scale for diffusion $T = \frac{{L_{pore}}^2}{D}$ through the TSNs is < 60 ms for the compounds
198 studied. As such TSNs will operate under quasi steady state conditions, given that the
199 timescale of diffusion through the TSN is very fast compared to any changes in concentration
200 in the much larger volumes of the maternal intervillous space and fetal capillary to either side.
201 There are differences in the placental permeability of different compounds from
202 literature, which could not be fully explained based on diffusivity and thus affected the
203 number of pores estimated, with higher estimated pore numbers for smaller molecules. One
204 explanation for this is that there may be more thinner pores available that only allow passage
205 of smaller molecules. However, we do not think that this is the explanation for what is
206 observed here. Paracellular diffusion across the placenta is size-selective, but the TSNs are
207 likely to be too wide to impose this size selectivity on smaller molecules. Physiological
208 estimates of placental pore sizes in rodents are in the order of 17 nm, which is consistent with
209 the thinnest regions of the nanopores described here and with the desmosome associated
210 channels we observed [15]. For comparison glucose is 1.5 nm long so would be expected to
211 diffuse freely though pores of this size. If the TSNs do not impose size selectivity, other
212 structures such as the trophoblast basal lamina or the capillary endothelium might, and
213 further research is required to understand this better [16].
214 Molecules such as IgG or nanoparticles such as ultrafine diesel exhaust could diffuse
215 into most regions of the TSNs, but the diameter would sterically hinder their transfer. TSN
216 diameter might be a significant barrier to the transfer of large molecules unless an additional
217 biological mechanism facilitates this transfer.
218 On the basal membrane TSNs opened adjacent to both basal lamina and
219 cytotrophoblast cells. TSNs opening to the basal lamina would provide the most direct
220 pathway to the fetal circulation. Substances diffusing through TSNs opening adjacent to
221 cytotrophoblast would have a less direct path to reach the fetus but these solutes could
222 interact with the cytotrophoblast themselves.
223 Further research is required to determine TSN densities in placental tissue. An initial
224 approximation for the TSN density was obtained by dividing the number of observed TSNs (10
225 continuous or 30 including continuous and near-continuous TSNs) by the imaged volume of
226 0.00000017 cm^3. This initial approximation for TSN density is 58 million TSNs per cm^3, and
227 including near-continuous TSNs is 162 million/cm^3. This estimate is in line with modelled
228 estimate of the number of TSNs required to mediate transfer of known paracellular markers
229 such as inulin and creatinine.
230 The 50 nm z-resolution is a potential technical limitation in this study. Firstly, it may
231 lead us to classify some continuous TSNs as near continuous and secondly could also affect

232 the accuracy of the geometric representation in the computational models affecting the
233 calculated permeability parameters. The use of focused ion beam scanning electron
234 microscopy could reduce z depth, but this approach has a smaller field of view making finding
235 TSNs more difficult.

236 The physiological role of TSNs is likely to include the maintenance of ionic and osmotic
237 homeostasis between mother and fetus. Diffusion of ions and bulk fluid flow would balance
238 osmotic and pressure gradients that could build up across an impermeable placenta. TSNs
239 may also facilitate the placental transfer of nutrients, such as glucose, with maternal to fetal
240 gradients to the fetus [17]. However, the physiological roles of TSNs may come at the cost of
241 allowing non-selective transfer of potentially harmful substances.

242 The presence of membrane-bound inclusions within the TSNs suggests their role could
243 be more complex than simply being pores for diffusion. The nanopore inclusions and
244 surrounding TSN membrane create a double membrane structure which show ultrastructural
245 similarities to autophagosomes [18]. Nanopore inclusions can be observed in a previous study
246 that sought to identify TSNs using lanthanum perfusion [7].

247 While the origin and nature of the inclusions remains unclear, in some cases they
248 appeared trophoblastic in origin. One inclusion appeared to be connected to the
249 syncytiotrophoblast by a stalk of cytoplasmic material which is consistent with
250 syncytiotrophoblast being pinched off into a nanopore to form an inclusion. If this
251 interpretation is correct this could potentially represent the initiation of autophagy or
252 material that will be shed from the placenta. In other cases, inclusions on the basal side of
253 the placenta were observed to be protrusions from underlying cytotrophoblast cells.

254 A rare feature associated with TSNs were desmosome associated nanopores which
255 could be observed arising from basal membrane folds [19], and within the cytoplasm but not
256 observed connecting to the microvillous membrane. The connect to dilations that appear
257 similar to, or are, the TSNs that are the main focus of this paper. It is possible that the TSNs
258 represent formation or breakdown of TSNs or that they are a separate class of nanopore that
259 intersect with TSNs. The desmosome associated nanopores have been observed previously in
260 2D TEM images where it was suggested that they are remnants of cytotrophoblast-
261 syncytiotrophoblast fusion. We cannot exclude this trophoblast fusion explanation, but in the
262 limited number of 3D examples we identified the structures were more like ribbon than a cell-
263 cell junctions [20]. Desmosome associated nanopores are very thin and so may not be visible
264 when the block is in the wrong orientation and so could be more common than they appear.

265 Cells that cross or penetrate epithelial barriers have been observed to express tight
266 junction proteins to facilitate movement through cell-cell junctions, and the desmosome
267 containing nanopores in the syncytiotrophoblast could provide a route and a mechanism by
268 which maternal or fetal cells could cross the syncytiotrophoblast [21, 22]. Images of
269 erythrocytes protruding through the syncytiotrophoblast are consistent with distensible
270 channels that could allow cell transfer [23].

271 There is considerable diversity in placental structures across species and given the
272 possibility that the syncytiotrophoblast has evolved independently in different branches of

273 the evolutionary tree, the diversity of TSNs (or similar structures) is of interest. To date, full
274 width trans-syncytial channels have only been described in the degu which has both short
275 direct channels in thin regions of syncytiotrophoblast and more complex channels connecting
276 infoldings of basal and apical surfaces [24]. The human TSNs had a distinct appearance but
277 were most similar to the more complex Degu channels, although longer and thinner. The
278 distribution of TSNs across species may inform their biological role and origins.
279 Identifying the molecular processes underlying TSN formation will be key to
280 understanding these structures. While TSNs may form by a unique mechanism, they are more
281 likely to co-opt at least some of the known molecular mechanisms that mediate endocytosis.
282 There are multiple endocytic processes, including clathrin and caveolin, micropinosomes or
283 CLIC/GEEC, which form tubular structures [25]. The CLIC/GEEC may be of particular interest
284 as these form tube-like structures [26].
285 In conclusion, this study has demonstrated the existence of TSNs providing a non-
286 selective diffusion pathway across the placenta. These TSNs may allow pharmacological
287 drugs, environmental toxins and even particulate pollutants across the syncytiotrophoblast.
288 Accurately determining the density of TSNs in healthy pregnancy is necessary to confirm the
289 capacity of TSNs to mediate transfer. Furthermore, establishing the density of TSNs in disease
290 may provide novel insights into disease processes.
291
292 **Acknowledgements**: This work was supported by BBSRC project grant BB/R002762/1.
293 Equipment in the Biomedical Imaging Unit was supported by MR/L012626/1 Southampton
294 Imaging under MRC UKRMP Funding.
295
296 **Competing interests**: The authors have no competing interests to declare

297 **References**

298 1. Dally A. Thalidomide: was the tragedy preventable? Lancet. 1998;351(9110):1197-9.
299 Epub 1998/06/27. doi: 10.1016/S0140-6736(97)09038-7. PubMed PMID: 9643709.
300 2. Lofthouse EM, Torrens C, Manousopoulou A, Nahar M, Cleal JK, O'Kelly IM, et al.
301 Ursodeoxycholic acid inhibits uptake and vasoconstrictor effects of taurocholate in human
302 placenta. FASEB journal : official publication of the Federation of American Societies for
303 Experimental Biology. 2019;33(7):8211-20. Epub 2019/03/30. doi: 10.1096/fj.201900015RR.
304 PubMed PMID: 30922127; PubMed Central PMCID: PMCPMC6593889.
305 3. Bove H, Bongaerts E, Slenders E, Bijnens EM, Saenen ND, Gyselaers W, et al. Ambient
306 black carbon particles reach the fetal side of human placenta. Nat Commun. 2019;10(1):3866.
307 Epub 2019/09/19. doi: 10.1038/s41467-019-11654-3. PubMed PMID: 31530803; PubMed
308 Central PMCID: PMCPMC6748955.
309 4. Lewis RM, Demmelmair H, Gaillard R, Godfrey KM, Hauguel-de Mouzon S, Huppertz
310 B, et al. The Placental Exposome: Placental Determinants of Fetal Adiposity and Postnatal
311 Body Composition. Annals of Nutrition and Metabolism. 2013;63(3):208-15. doi:
312 10.1159/000355222. PubMed PMID: WOS:000329057400005.
313 5. Thornburg KL, Burry KJ, Adams AK, Kirk EP, Faber JJ. Permeability of placenta to inulin.
314 American journal of obstetrics and gynecology. 1988;158(5):1165-9. Epub 1988/05/01. doi:
315 10.1016/0002-9378(88)90246-3. PubMed PMID: 3369499.
316 6. Bain MD, Copas DK, Taylor A, Landon MJ, Stacey TE. Permeability of the human
317 placenta in vivo to four non-metabolized hydrophilic molecules. The Journal of physiology.
318 1990;431:505-13. PubMed PMID: 2129229; PubMed Central PMCID: PMCPMC1181787.
319 7. Kertschanska S, Kosanke G, Kaufmann P. Pressure dependence of so-called
320 transtrophoblastic channels during fetal perfusion of human placental villi. Microscopy
321 research and technique. 1997;38(1-2):52-62. doi: 10.1002/(SICI)1097-
322 0029(19970701/15)38:1/2<52::AID-JEMT7>3.0.CO;2-W. PubMed PMID: 9260837.
323 8. Brownbill P, Mahendran D, Owen D, Swanson P, Thornburg KL, Nelson DM, et al.
324 Denudations as paracellular routes for alphafetoprotein and creatinine across the human
325 syncytiotrophoblast. American journal of physiology Regulatory, integrative and comparative
326 physiology. 2000;278(3):R677-83. PubMed PMID: 10712288.
327 9. Cleal JK, Glazier JD, Ntani G, Crozier SR, Day PE, Harvey NC, et al. Facilitated
328 transporters mediate net efflux of amino acids to the fetus across the basal membrane of the
329 placental syncytiotrophoblast. The Journal of physiology. 2011;589(4):987-97. doi:
330 10.1113/jphysiol.2010.198549. PubMed PMID: WOS:000287743400026.
331 10. Lofthouse EM, Cleal JK, O'Kelly IM, Sengers BG, Lewis RM. Estrone sulphate uptake by
332 the microvillous membrane of placental syncytiotrophoblast is coupled to glutamate efflux.
333 Biochem Biophys Res Commun. 2018;506(1):237-42. Epub 2018/10/23. doi:
334 10.1016/j.bbrc.2018.10.074. PubMed PMID: 30343886.
335 11. Firan M, Bawdon R, Radu C, Ober RJ, Eaken D, Antohe F, et al. The MHC class I-related
336 receptor, FcRn, plays an essential role in the maternofetal transfer of gamma-globulin in
337 humans. Int Immunol. 2001;13(8):993-1002. Epub 2001/07/27. doi:
338 10.1093/intimm/13.8.993. PubMed PMID: 11470769.
339 12. Iqbal M, Audette MC, Petropoulos S, Gibb W, Matthews SG. Placental drug
340 transporters and their role in fetal protection. Placenta. 2012;33(3):137-42. Epub
341 2012/01/24. doi: 10.1016/j.placenta.2012.01.008. PubMed PMID: 22265855.
342 13. Gruber MM, Hirschmugl B, Berger N, Holter M, Radulovic S, Leitinger G, et al. Plasma
343 proteins facilitates placental transfer of polystyrene particles. J Nanobiotechnology.

344 2020;18(1):128. Epub 2020/09/11. doi: 10.1186/s12951-020-00676-5. PubMed PMID:
345 32907583; PubMed Central PMCID: PMCPMC7487953.
346 14. Sibley CP. Understanding placental nutrient transfer--why bother? New biomarkers of
347 fetal growth. The Journal of physiology. 2009;587(Pt 14):3431-40. doi:
348 10.1113/jphysiol.2009.172403. PubMed PMID: 19417095; PubMed Central PMCID:
349 PMC2742272.
350 15. Stulc J. Extracellular transport pathways in the haemochorial placenta. Placenta.
351 1989;10(1):113-9. Epub 1989/01/01. PubMed PMID: 2654915.
352 16. Harris SE, Matthews KS, Palaiologou E, Tashev SA, Lofthouse EM, Pearson-Farr J, et al.
353 Pericytes on placental capillaries in terminal villi preferentially cover endothelial junctions in
354 regions furthest away from the trophoblast. Placenta. 2021;104:1-7. Epub 2020/11/16. doi:
355 10.1016/j.placenta.2020.10.032. PubMed PMID: 33190063; PubMed Central PMCID:
356 PMCPMC7921774.
357 17. Day PE, Cleal JK, Lofthouse EM, Hanson MA, Lewis RM. What factors determine
358 placental glucose transfer kinetics? Placenta. 2013;34(10):953-8. doi:
359 10.1016/j.placenta.2013.07.001. PubMed PMID: WOS:000330331500016.
360 18. Mizushima N, Yoshimori T, Levine B. Methods in mammalian autophagy research. Cell.
361 2010;140(3):313-26. Epub 2010/02/11. doi: 10.1016/j.cell.2010.01.028. PubMed PMID:
362 20144757; PubMed Central PMCID: PMCPMC2852113.
363 19. Tashev SA, Parsons D, Hillman C, Harris S, Lofthouse EM, Goggin P, et al. Folding of the
364 syncytiotrophoblast basal plasma membrane increases the surface area available for
365 exchange in human placenta. Placenta. 2022;117:57-63. Epub 20211104. doi:
366 10.1016/j.placenta.2021.11.002. PubMed PMID: 34768170.
367 20. Jones CJ, Fox H. Ultrastructure of the normal human placenta. Electron Microsc Rev.
368 1991;4(1):129-78. PubMed PMID: 1873486.
369 21. Rescigno M, Urbano M, Valzasina B, Francolini M, Rotta G, Bonasio R, et al. Dendritic
370 cells express tight junction proteins and penetrate gut epithelial monolayers to sample
371 bacteria. Nat Immunol. 2001;2(4):361-7. Epub 2001/03/29. doi: 10.1038/86373. PubMed
372 PMID: 11276208.
373 22. Murrieta-Coxca JM, Aengenheister L, Schmidt A, Markert UR, Buerki-Thurnherr T,
374 Morales-Prieto DM. Addressing microchimerism in pregnancy by ex vivo human placenta
375 perfusion. Placenta. 2021;117:78-86. Epub 2021/11/14. doi: 10.1016/j.placenta.2021.10.004.
376 PubMed PMID: 34773744.
377 23. Palaiologou E, Goggin P, Chatelet DS, Lofthouse EM, Torrens C, Sengers BG, et al. Serial
378 block-face scanning electron microscopy of erythrocytes protruding through the human
379 placental syncytiotrophoblast. Journal of anatomy. 2017;231(4):634-7. Epub 2017/07/18. doi:
380 10.1111/joa.12658. PubMed PMID: 28714092; PubMed Central PMCID: PMCPMC5603844.
381 24. King BF. Ultrastructural evidence for transtrophoblastic channels in the
382 hemomonochorial placenta of the degu (Octodon degus). Placenta. 1992;13(1):35-41. Epub
383 1992/01/01. PubMed PMID: 1502135.
384 25. Cooke LDF, Tumbarello DA, Harvey NC, Sethi JK, Lewis RM, Cleal JK. Endocytosis in the
385 placenta: An undervalued mediator of placental transfer. Placenta. 2021;113:67-73. Epub
386 2021/05/18. doi: 10.1016/j.placenta.2021.04.014. PubMed PMID: 33994009.
387 26. Ferreira APA, Boucrot E. Mechanisms of Carrier Formation during Clathrin-
388 Independent Endocytosis. Trends Cell Biol. 2018;28(3):188-200. Epub 2017/12/16. doi:
389 10.1016/j.tcb.2017.11.004. PubMed PMID: 29241687.

390 27. Palaiologou E, Etter O, Goggin P, Chatelet DS, Johnston DA, Lofthouse EM, et al.
391 Human placental villi contain stromal macrovesicles associated with networks of stellate cells.
392 Journal of anatomy. 2020;236(1):132-41. Epub 2019/09/13. doi: 10.1111/joa.13082. PubMed
393 PMID: 31512233.
394 28. Atkinson DE, Robinson NR, Sibley CP. Development of passive permeability
395 characteristics of rat placenta during the last third of gestation. The American journal of
396 physiology. 1991;261(6 Pt 2):R1461-4. Epub 1991/12/01. doi:
397 10.1152/ajpregu.1991.261.6.R1461. PubMed PMID: 1750569.
398 29. Cleal JK, Brownbill P, Godfrey KM, Jackson JM, Jackson AA, Sibley CP, et al.
399 Modification of fetal plasma amino acid composition by placental amino acid exchangers in
400 vitro. The Journal of physiology. 2007;582(Pt 2):871-82. doi: 10.1113/jphysiol.2007.130690.
401 PubMed PMID: 17478537; PubMed Central PMCID: PMCPMC2075319.
402 30. Edwards D, Jones CJ, Sibley CP, Nelson DM. Paracellular permeability pathways in the
403 human placenta: a quantitative and morphological study of maternal-fetal transfer of
404 horseradish peroxidase. Placenta. 1993;14(1):63-73. doi: 10.1016/s0143-4004(05)80249-8.
405 PubMed PMID: 8456090.
406 31. Brownbill P, Edwards D, Jones C, Mahendran D, Owen D, Sibley C, et al. Mechanisms
407 of alphafetoprotein transfer in the perfused human placental cotyledon from uncomplicated
408 pregnancy. The Journal of clinical investigation. 1995;96(5):2220-6. doi: 10.1172/JCI118277.
409 PubMed PMID: 7593608; PubMed Central PMCID: PMCPMC185872.
410 32. Collins MC, Ramirez WF. Transport through polymeric membranes. J Phys Chem
411 1979;83:2294–301. doi: https://doi.org/10.1021/j100480a022.
412

Figures and tables

Table 1: Estimated number of pores per gram required to explain the experimentally observed placental permeability surface area products.

	MW (da)	D ($m^2\ s^{-1}$)	PS_{pore} ($m^3\ s^{-1}$)	$PS_{placenta}$ ($m^3\ s^{-1}\ g^{-1}$)	number of pores (g^{-1})
Inulin*	6179	2.6×10^{-10}	2.20×10^{-18}	0.28×10^{-10}	13×10^{6}
CrEDTA*	344	7.0×10^{-10}	5.92×10^{-18}	1.06×10^{-10}	18×10^{6}
Mannitol*	182	9.9×10^{-10}	8.37×10^{-18}	2.50×10^{-10}	30×10^{6}
Creatinine**	113	12.9×10^{-10}	10.9×10^{-18}	4.00×10^{-10}	37×10^{6}

*Placental permeability surface area product data taken from Bain *et al.* (1990) [6] and diffusion coefficients from Atkinson *et al.* (1991) [28]. ** Placental permeability surface area product based on the average of values from Cleal *et al.* (2007)[29], Edwards et al 1993 [30] & Brownbill et al 1995 [31] and diffusion coefficient from Collins *et al.* (1979) [32].

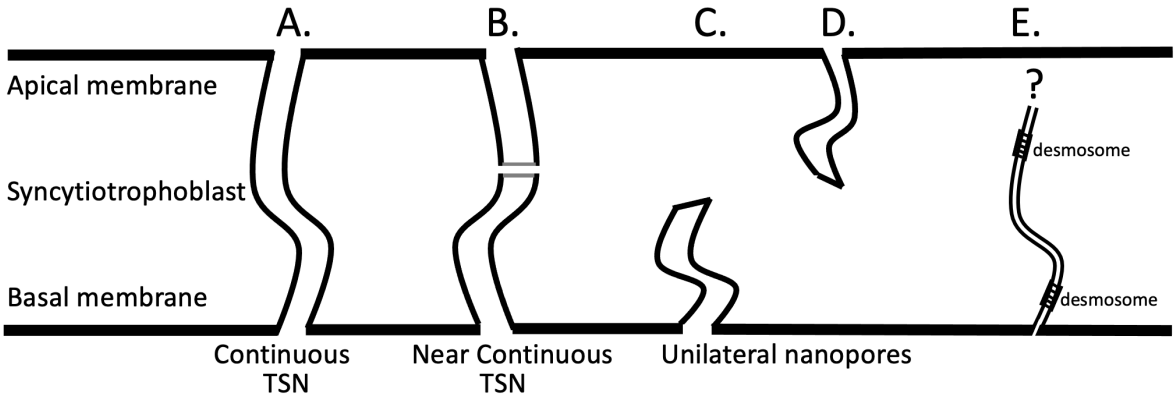

Figure 1, Classification of nanopores found in human placental syncytiotrophoblast. A) continuous TSNs connecting the apical and basal membrane without any breaks. **B)** near-continuous TSNs with sections connected to the apical and basal plasma membranes but contained discontinuities where no clear connection could be observed but the ends of the discontinuous sections were adjacent. **C & D)** Unilateral nanopores were ultrastructurally similar to TSNs but opened from either the apical or basal plasma membrane but without any apparent connection to the opposing membrane. **E)** Desmosome associated nanopores were also observed arising from the basal membrane but none of these could be observed connecting to the apical membrane.

434

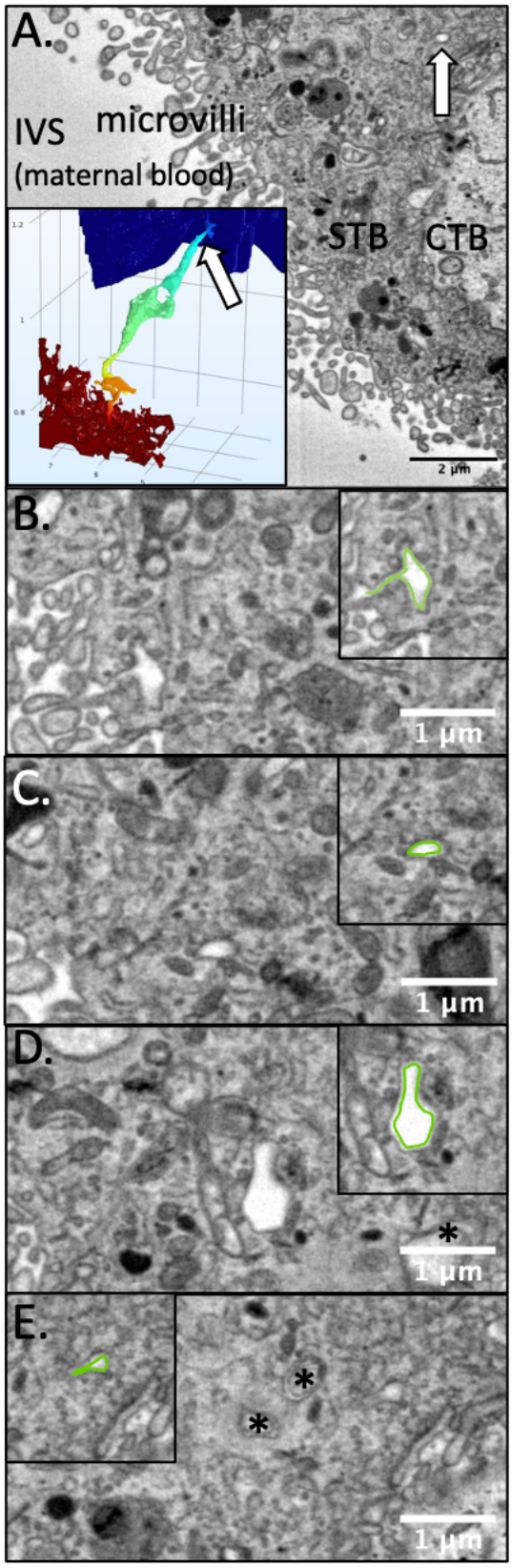

Figure 2, SBF SEM serial sectioning allows identification of TSNs crossing the human placental syncytiotrophoblast. A) An SBF SEM image showing a cross section of the syncytiotrophoblast (STB) from the maternal intervillous space (IVS) to the underlying cytotrophoblast (CTB). Within this image a cross section of a nanopore can be seen (white arrow) illustrating how difficult it would be to identify these structures from individual 2D images. The inset shows the nanopore reconstructed in 3D from 44 consecutive sections with the white arrow indicating where the section comes from and modelled solute concentration indicated by colour from high (red) to low (blue). **B)** the apical opening of the TSN with the inset showing this highlighted in green. **C)** A thin region of nanopore with the inset showing this highlighted in green. **D)** a dilated region of the nanopore with the inset showing this highlighted in green. In B, C and D the nanopore has a low electron density consistent with a fluid filled pore **E)** A region of nanopore where the lumen has a higher electron density than in other regions. The inset showing this cross section of the nanopore highlighted in green. This region is close to the end of the nanopore and the cytotrophoblast boundary can be seen bottom left. * Indicates inclusions in other TSNs in the section. A movie showing the nanopore reconstructed in 3D and another movie with the nanopore lumen highlighted in sequential sections can be seen in the supplemental material.

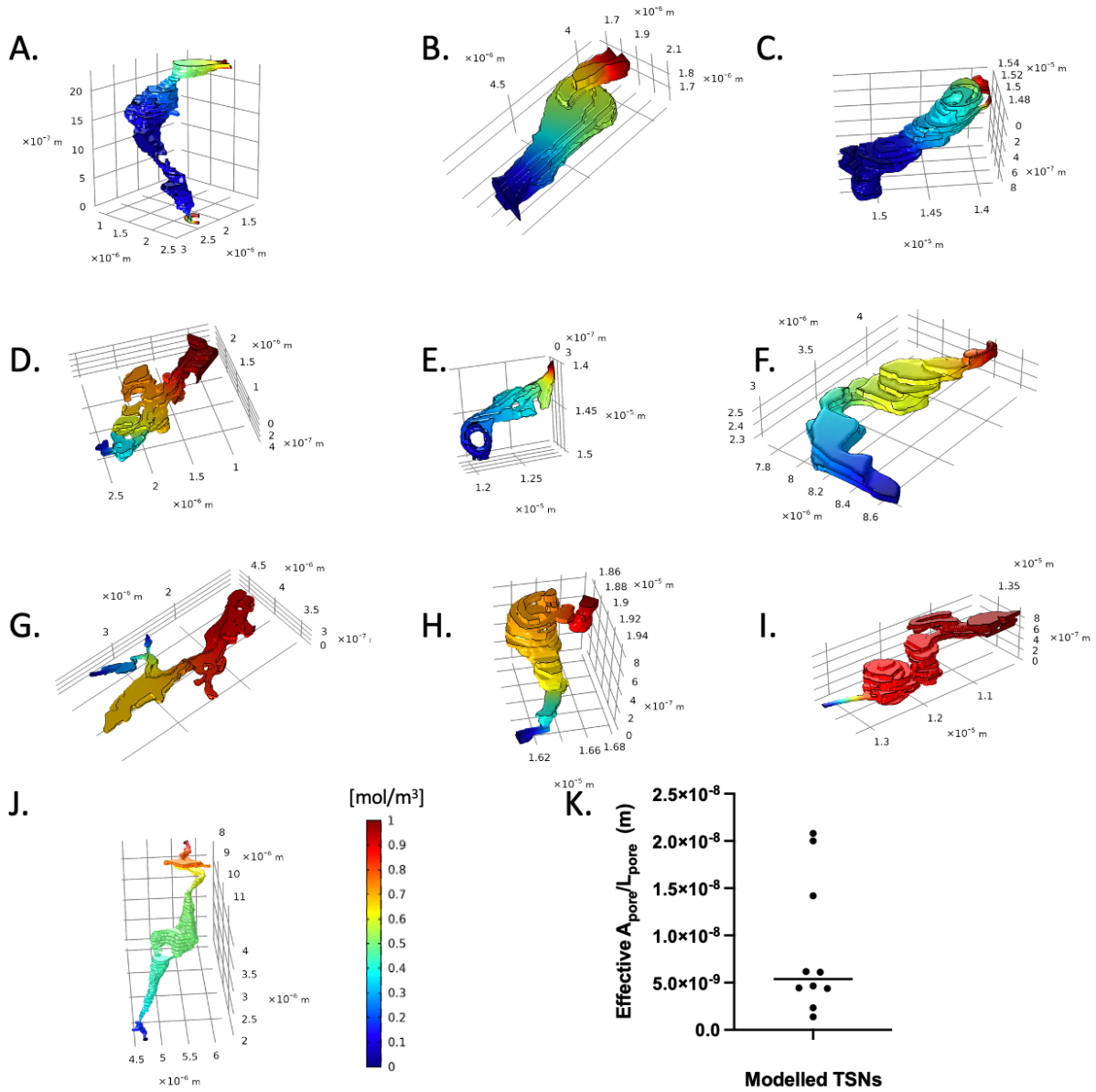

Figure 3, **Modelled solute concentration gradients within the continuous TSNs.** High concentrations (red) were applied to the maternal facing TSN opening, and concentration gradients are shown for diffusion through the channel. The molecular flux associated with these gradients was used to calculate the effective cross sectional surface area used to calculate permeability. **A-J)** show the nanopores presented in order of calculated permeability from highest to lowest. The apical opening is presented on top right and basal openings on the bottom or left. The TSN shown in A is a double pore with four apical and basal openings and a connection on the basal side which accounts for its higher permeability despite its longer length. Blind ends are present in D, I and G. TSN A has two openings to the microvillous membrane and two openings to the basal membrane of the syncytiotrophoblast. **J)** shows a scatterplot showing the distribution of permeabilities with the line indicating the median value.

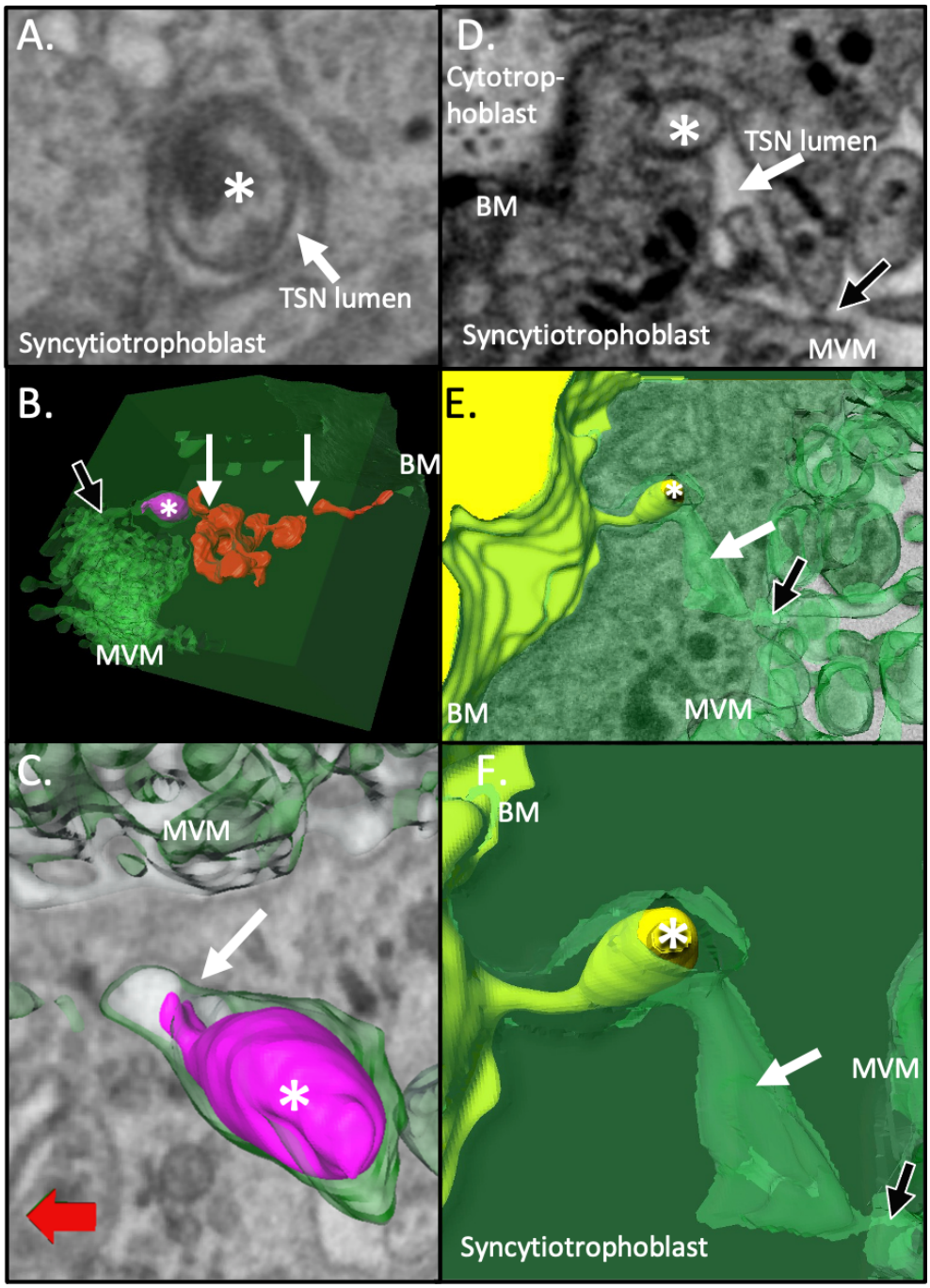

Figure 4, **Examples of TSN inclusions formed from engulfed syncytiotrophoblast or villous cytotrophoblast. A-C**) An example of an apical nanopore inclusion (highlighted by an *) which in 3D can be seen to be budding off the syncytiotrophoblast within the nanopore. **A)** shows a SBF SEM image containing a cross section of the TSN inclusion. **B)** shows the pink inclusion reconstructed in 3D within the TSN formed from green syncytiotrophoblast. This inclusion lies within a complex near-continuous TSN which, apart from regions around the inclusion, is shown in red. This TSN has discontinuities indicated by white arrows but gives the appearance of being part of a trans-syncytial network. A black arrow indicates the apical opening of this TSN. **C)** shows a higher magnification image of the pink inclusion and the connection to the green syncytiotrophoblast is indicted by a white arrow. **D-F)** An example of a TSN inclusion, which in 3D is seen to be derived from underlying villous cytotrophoblast. In panels D-F an * indicates the inclusion, white arrows indicate the lumen of the TSN and black arrow indicates the apical opening of the TSN on the microvillous membrane. **D)** shows a 2D SBF SEM image of the syncytiotrophoblast containing a cross section of a TSN and an inclusion containing an inclusion. **E)** shows the 3D structure of this region with the villous cytotrophoblast in yellow and the syncytiotrophoblast in green. **F)** shows a higher magnification image of the structure of the villous cytotrophoblast derived inclusion and the TSN channel. BM and MVM are the basal membrane and apical microvillous membranes of the syncytiotrophoblast.

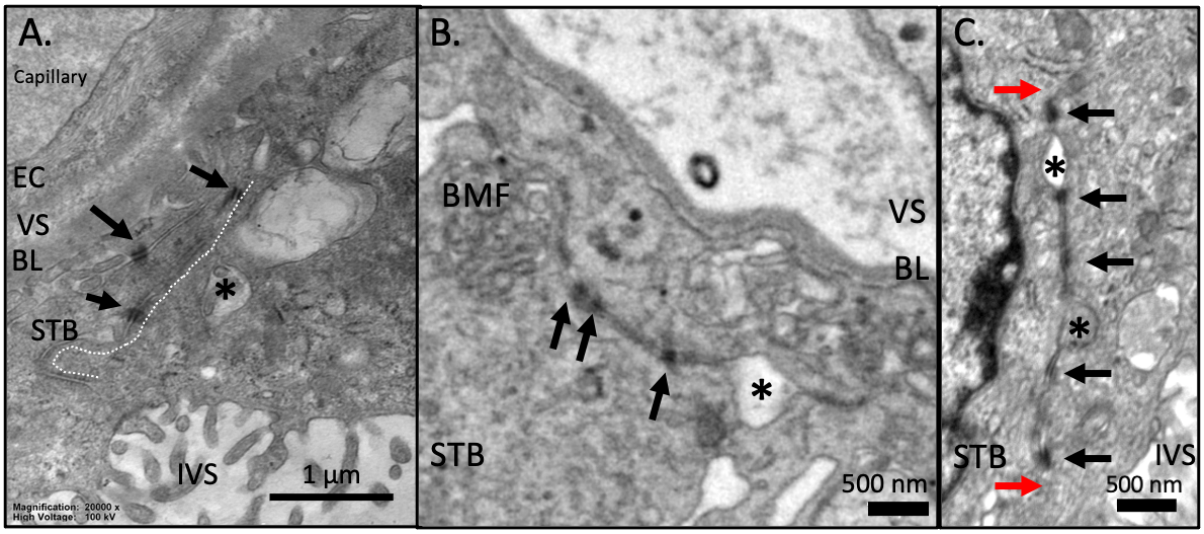

Figure 5, Desmosome associated nanopores. A) a TEM image of a desmosome associated nanopore traversing most of the width of the syncytiotrophoblast (white dotted line). The desmosomes are indicated by black arrows. This type of nanopore was associated with dilations typical of the TSNs described in the previous figures (indicated by *). **B)** an SBF SEM image of a desmosome associated nanopore connecting basal membrane folds to a TSN like opening (indicated by *). **C)** A TEM image of a desmosome associated nanopore which begins and ends in the same field of view (red arrows). This demonstrates that these structures are not a cell-cell junction, as if this were the case it would need to intersect 2 sides of the image or be a circle. This channel contains an empty TSN like dilation (indicated by the top*) and one which contains inclusion material (indicated by the bottom*). EC = endothelial cell, VS = villous stroma, BL = basal lamina, STB = syncytiotrophoblast, BMF = basal membrane folds. IVS = intervillous space.